ADVANCED FUNCTIONAL MATERIALS
www.afm-journal.de

Materials Views
www.MaterialsViews.com

Non-stoichiometry in Oxide Thin Films: A Chemical Capacitance Study of the Praseodymium-Cerium Oxide System

*Di Chen, Sean R. Bishop, and Harry L. Tuller**

While the properties of functional oxide thin films often depend strongly on their oxygen stoichiometry, there have been few ways to extract this information reliably and in situ. In this work, the derivation of the oxygen non-stoichiometry of dense $Pr_{0.1}Ce_{0.9}O_{2-\delta}$ thin films from an analysis of chemical capacitance obtained by impedance spectroscopy is described. Measurements are performed on electrochemical cells of the form $Pr_{0.1}Ce_{0.9}O_{2-\delta}$/$Y_{0.16}Zr_{0.84}O_{1.92}$/$Pr_{0.1}Ce_{0.9}O_{2-\delta}$ over the temperature range of 450 to 800 °C and oxygen partial pressure range of 10^{-5} to 1 atm O_2. With the aid of a defect equilibria model, approximations relate chemical capacitance directly to non-stoichiometry, without need for fitting parameters. The calculated non-stoichiometry allows extraction of the thermodynamic constants defining defect generation. General agreement of these constants with bulk values derived by thermogravimetric analysis is found, thereby confirming the suitability of this technique for measuring oxygen non-stoichiometry of thin oxide films. Potential sources of error observed in earlier chemical capacitance studies on perovskite structured oxide films are also discussed.

1. Introduction

Oxides are increasingly used in the form of thin films at elevated temperatures and varied gas compositions in, for example, miniaturized gas sensors and micro solid oxide fuel cells (μSOFCs).[1,2] Additionally, the ability to reproducibly prepare films with well-defined microstructure, thickness, orientation, crystallinity,[3] and composition has enabled a more careful and systematic investigation of their transport properties.[4,5] While many features of these films can be readily measured (e.g., in-plane and cross-plane electrical conductivity;[6,7] surface composition),[8] a key limitation has been the ability to measure and monitor changes in oxygen stoichiometry–a factor strongly tied to, among other physical properties, electronic conductivity and film strain.[9] This is a consequence of the very small mass changes involved when dealing with thin films, precluding the use of more traditional thermogravimetric techniques, though resonant crystal microbalance studies have been attempted with limited success.[10]

A number of investigators have advanced the use of an in situ electrochemical method, via impedance spectroscopy (IS), in which one measures the chemical capacitance of the material, in film or bulk form, and relates it to the oxygen content using thermodynamic principles. In some cases, the oxygen stoichiometry measured this way does not agree well with that of the bulk, determined by thermogravimetric analysis (TGA) or coulometric titration. This discrepancy is suspected to arise from lattice mismatch stresses in the film or other gas/solid and film/substrate interfacial interactions. For example, a reduced oxygen stoichiometry content has been reported in thin films of $La_{1-x}Sr_xCoO_{3-\delta}$ as compared to the bulk, while others have reported opposite behavior.[11–13] On the other hand, defect formation energies for thin film $Sm_{0.15}Ce_{0.85}O_{2-\delta}$ and oxygen non-stoichiometries for thin film $Gd_{0.1}Ce_{0.9}O_{2-\delta}$ and $La_2NiO_{4+\delta}$ extracted from chemical capacitance measurements were found to be comparable to bulk values.[14–16] In the former an additional, presumably interfacial, capacitive contribution was observed and an analysis technique was developed to isolate this contribution. In the latter study of $La_2NiO_{4+\delta}$, the results were characterized by a limited data set restricted to only a single pO_2.

In this study, praseodymium-cerium oxide ($Pr_xCe_{1-x}O_{2-\delta}$; PCO), a potential three way catalyst–oxygen storage material,[9] and solid oxide fuel cell (SOFC) cathode,[17] was selected for study, given its surprisingly high levels of oxygen non-stoichiometry even under oxidizing (e.g., air) conditions (as compared to the much lower reducibility of $Sm_{0.15}Ce_{0.85}O_{2-\delta}$ and $Gd_{0.1}Ce_{0.9}O_{2-\delta}$), and its well characterized defect chemistry (in the bulk).[18] In our previous work,[17] we studied the impedance of PCO thin film electrodes deposited onto yttria stabilized zirconia ($Y_{0.16}Zr_{0.84}O_{1.92}$; YSZ) single crystal electrolytes under temperature and atmosphere conditions typical of an SOFC cathode and obtained the following results: (i) the rate determining step for the oxygen reduction reaction is a process involving oxygen surface exchange across the gas/PCO interface

D. Chen, Prof. S. R. Bishop, Prof. H. L. Tuller
Department of Materials Science and Engineering
Massachusetts Institute of Technology
Cambridge, MA 02139, USA
E-mail: tuller@mit.edu
Prof. S. R. Bishop
International Institute for Carbon Neutral Energy Research (WPI-I2CNER)
Kyushu University
Nishi-ku Fukuoka 819-0395, Japan

DOI: 10.1002/adfm.201202104

with (ii) no measurable barrier for transfer of oxygen across the electrolyte/electrode interface. In this paper, the oxygen non-stoichiometry (δ) in $Pr_{0.1}Ce_{0.9}O_{2-\delta}$ thin films is investigated by analysis of the chemical capacitance derived from IS and compared to δ reported previously for the bulk with the same cation composition.[18] The derivation of absolute oxygen vacancy concentration using a relatively simple defect equilibria based analysis is developed, directly relating chemical capacitance to δ without any fitting parameters. With these absolute values of δ thus evaluated, δ is then determined from chemical capacitance in regions extending away from the simplified defect equilibria approximations.

2. Theory

2.1. Defect Chemistry of $Pr_{0.1}Ce_{0.9}O_{2-\delta}$

In our recent paper, measurements of oxygen non-stoichiometry and electrical conductivity performed on bulk $Pr_{0.1}Ce_{0.9}O_{2-\delta}$ were presented, and on this basis, a defect equilibrium model was developed.[18] In PCO, oxygen vacancies are introduced in the material through the following defect reaction written in Kröger–Vink notation and followed by the corresponding mass action, or equilibrium, equation:

$$2Pr_{Ce}^{\times}+O_O^{\times} \leftrightarrow 2Pr_{Ce}^{'}+V_O^{\bullet\bullet}+1/2O_2(g) \tag{1}$$

$$\frac{[Pr'_{Ce}]^2\left[V_O^{\bullet\bullet}\right] pO_2{}^{1/2}}{\left[Pr_{Ce}^{\times}\right]^2\left[O_O^{\times}\right]} = k^{\circ}_{r,Pr}\exp\left(\frac{-H_{r,Pr}}{kT}\right) = K_{r,Pr} \tag{2}$$

where $O_O^{\times}$,$V_O^{\cdot\cdot}$, Pr'_{Ce}, and $Pr_{Ce}{}^{\times}$ are oxide ions on oxygen sites, doubly positive charged (with respect to the lattice) oxygen vacancies, Pr^{3+}, and Pr^{4+}, respectively. In the equilibrium equation, $k^{\circ}_{r,\,Pr}$ is a pre-exponential term and $H_{r,Pr}$ is the enthalpy for the reaction. When Pr is in sufficiently high concentrations (>5 mol%), it forms a narrow impurity band (partially filled at high pO_2) that supports mixed ionic electronic conduction (MIEC), a common criteria for high performance SOFC cathodes.[19]

The condition for charge neutrality is given by

$$\left[Pr'_{Ce}\right] = 2\left[V_O^{\bullet\bullet}\right] \tag{3}$$

with the understanding that the concentrations of holes, reduced Ce, and oxygen interstitials are negligibly small under the present conditions. Mass and site conservation reactions are given by

$$\left[Pr'_{Ce}\right]+\left[Pr_{Ce}^{\times}\right]=[Pr_{Ce}]_{total}=0.1[Pr_{0.1}Ce_{0.9}O_{2-\delta}] \tag{4}$$

$$\left[V_O^{\bullet\bullet}\right]+\left[O_O^{\times}\right]=2[Pr_{0.1}Ce_{0.9}O_{2-\delta}] \tag{5}$$

where $[Pr_{0.1}Ce_{0.9}O_{2-\delta}]$ is the concentration of PCO in #/cm^{-3}. Additionally, the enthalpy of reduction of both undoped and Pr doped ceria have been reported to vary linearly with non-stoichiometry (δ) as:[18,20,21]

$$H_{r,Pr} = H^{o}_{r,Pr} + f\delta \tag{6}$$

with $\delta = [V_O^{\cdot\cdot}]/[Pr_{0.1}Ce_{0.9}O_2]$.

2.2. Relationship between δ and C_{chem}

Chemical capacitance (C_{chem}) is a measure of a chemical storage capacity of a material under a potential, in this case the formation/annihilation of $V_O^{\cdot\cdot}$ and Pr'_{Ce}.[11,22,23] Following the derivation of Nakamura et al., capacitance is expressed as[14]

$$C = \frac{dQ}{dE} \tag{7}$$

where Q is the charge stored for a given electrical potential, E. For C_{chem}, dQ is replaced by the amount of stored chemical species

$$dQ_{chem} = 2qV_{film}d\left[V_O^{\bullet\bullet}\right] \tag{8}$$

where q and V_{film} are the elementary charge of an electron and volume of the film, respectively, with the factor of two representing the two charges per vacancy. Equation (8) is valid for uniform concentration of defects within a film, as in the case where surface oxygen exchange limits oxygen transport in and out of the film (as opposed to bulk diffusion limitation). dE is replaced by the Nernst potential for oxygen.

$$dE_{Nernst} = -\frac{kT}{4qpO_2}dpO_2 \tag{9}$$

where k and T are the Boltzmann constant and temperature, respectively, with ideal behavior of oxygen assumed. Substituting Equations (8) and (9) into Equation (7) leads to the expression for C_{chem} as below.

$$C_{chem} = -\frac{8q^2V_{film}}{kT}\left(pO_2\frac{\partial[V_O^{\bullet\bullet}]}{\partial pO_2}\right) \tag{10}$$

The film oxygen vacancy concentration can be estimated at each pO_2 through integration of Equation (10) with respect to pO_2 as

$$[V_O^{\bullet\bullet}](pO_2) = \frac{kT}{8q^2V_{film}}\int C_{chem}d\ln pO_2 + [V_O^{\bullet\bullet}](pO_2^{\circ}) \tag{11}$$

where pO_2° is a reference oxygen pressure at which $[V_O^{\cdot\cdot}]$ is known. As shown later, $[V_O^{\bullet\bullet}](pO_2^{\circ})$ is determined using simple approximations of the defect equilibria relationship, Equation (2).

3. Results and Discussion

3.1. Film Characterization

The XRD pattern obtained from 2θ–ω coupled scans of the YSZ single crystal, with and without the PCO film, exhibited only (001) fluorite peaks demonstrating that the PLD deposited PCO films were fluorite structured with a highly (001) oriented texture. Surface analysis by AFM showed a dense and smooth

film with apparent grain size of approximately 50 nm and surface roughness of approximately 0.5 nm. Details of film characterization are discussed elsewhere.[17]

3.2. Rate-Determining Step and Equivalent Circuit

Figure 1 shows typical impedance spectra obtained for both the asymmetric and symmetric cells at 650 °C in air. As shown in the inset, the spectra are represented by a resistor in series with *R//Q* circuits (*R//Q*: a resistor in parallel with a constant phase element [CPE]). CPEs are used to take into account any inhomogeneities in the electrodes resulting in "depressed" arcs not well represented by ideal capacitors.[19] The impedance of a CPE is given by

$$Z = \frac{1}{Q(i\omega)^{n_q}} \tag{12}$$

where ω, i, and n_q are angular frequency, $\sqrt{-1}$, and a factor related to the deviation from ideal capacitance. An equivalent capacitance is derived from Q using the following equation[24]

$$C = Q\omega_{max}^{n_q-1} = (R^{1-n_q}Q)^{1/n_q} \tag{13}$$

The equivalent circuit fits are observed to represent the data well. As discussed in the authors' previous work, different film geometries were used to determine the origin of each component in the circuit.[17] R_{YSZ} reflects the series YSZ ohmic contribution to the overall cell impedance, R_{Ag} and C_{Ag} arise from the porous Ag electrode in the asymmetric cell, and R_{PCO} is the electrode resistance at the PCO/gas interface, limited by oxygen surface exchange kinetics. Lastly, C_{PCO} is the chemical capacitance of the PCO film, being linearly proportional to film volume (see Equation (10)). Typical n_q values near unity (0.979–0.997 were measured) for Q corresponding to C_{PCO} (see Equation (13)) demonstrate near ideal capacitance. Additionally, the relatively large C_{PCO} values (e.g., 1–30 mF cm^{-2}) are indicative of chemical capacitance, as reported for other thin film MIEC systems.[25,26] **Figure 2** shows C_{PCO} plotted as a function of film thickness. The fact that the linear fit passes through the origin confirms the absence of the additional interfacial capacitance previously observed in thin film $Sm_{0.15}Ce_{0.85}O_{2-\delta}$.[15]

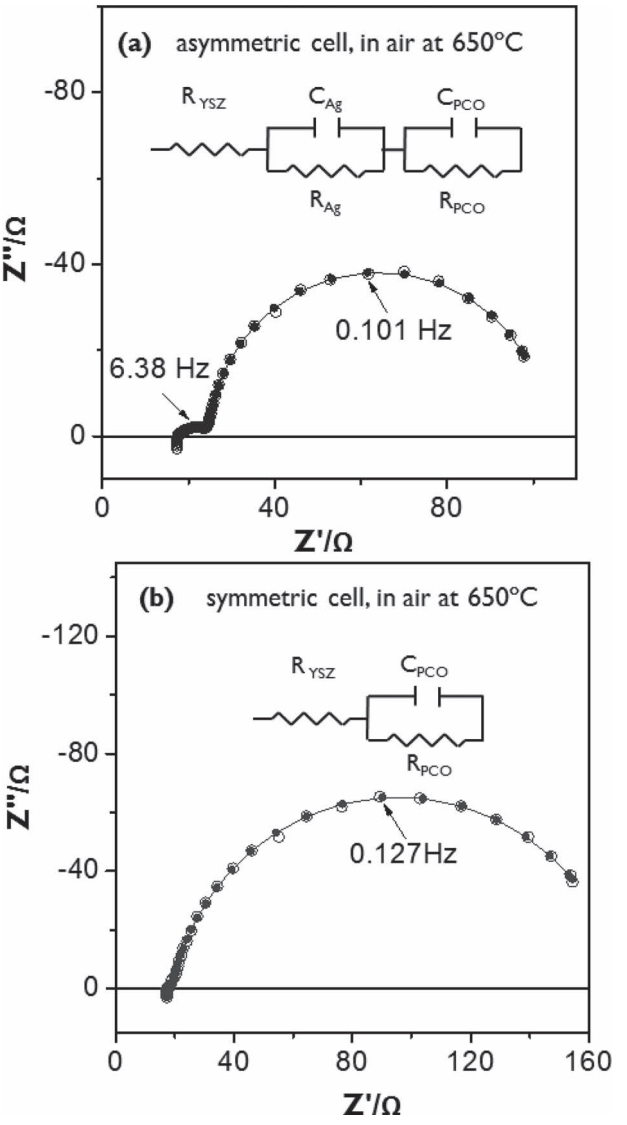

Figure 1. Typical impedance spectra of a) an asymmetric cell of PCO/YSZ/Ag and b) a symmetric cell of PCO/YSZ/PCO at 650 °C in air (modified from ref. [17]), where variables are defined in the text. The open circles are the experimental data while the solid data points are the equivalent circuit fit with frequencies at each peak indicated. Film thickness is 249 nm.

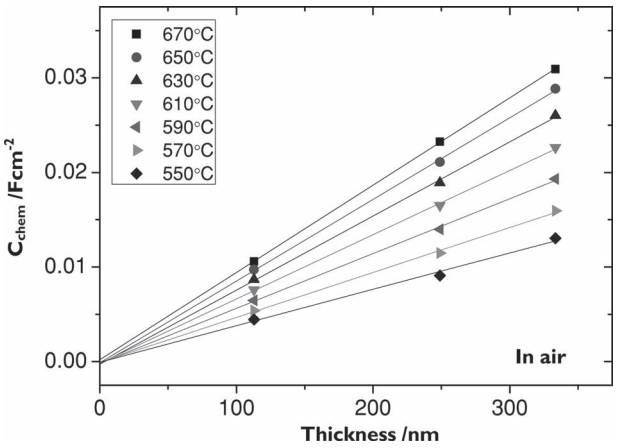

Figure 2. Thickness dependence of C_{PCO}, measured at different temperatures in air using the asymmetric cell configuration.

3.3. Estimation of Defect Equilibrium Parameters

Figure 3 shows both concentration of defects and C_{chem} as a function of pO_2, calculated using the above derived defect equilibrium model and Equation (10), respectively. In the figure, one observes an increase in vacancy and Pr'_{Ce} concentration with decreasing pO_2, corresponding to reduction and depletion

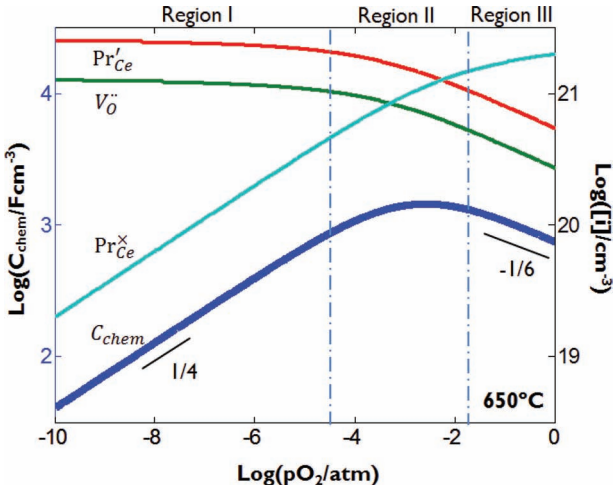

Figure 3. Predicted volume-specific C_{chem} (thick solid line) and defect concentrations (thin solid lines) at 650 °C derived from PCO defect equilibria parameters obtained for bulk specimens.[18] Insignificant reduction of cerium ions assumed (predicted to occur only at considerably lower pO_2).

of $Pr_{Ce}^{\times}$. Ultimately, $[V_O^{\cdot\cdot}]$ approximately saturates to half the total amount of Pr ($[Pr_{Ce}]_{total}$). At much lower pO_2 (not shown), Ce will begin reducing, resulting in a further increase of $[V_O^{\cdot\cdot}]$.

Interestingly, during this reduction process, the predicted C_{chem} exhibits three notable features: a power law dependence (slope = −1/6) in region III; a maximum, or peak, in region II; and a power law dependence of opposite sign (slope = 1/4) in region I. The peak in C_{chem} corresponds to the maximum change in $[V_O^{\cdot\cdot}]$ with pO_2 (approximately where $[Pr_{Ce}^{\times}]/[Pr'_{Ce}]$ is unity) and the power law dependences arise from Brouwer approximations of the defect equilibria, used later to derive $[V_O^{\bullet\bullet}](pO_2^{\circ})$. As shown in the next discussion, all three features exist in the measured C_{chem}, serving as an excellent demonstration of its relationship with defect equilibria.

In **Figure 4**, the experimentally derived values for C_{chem} of the symmetric cell are plotted as a function of pO_2 for a series of isotherms (450 to 800 °C). The solid curves represent the calculated values of C_{chem}, derived with the aid of Equation (10) and using $[V_O^{\cdot\cdot}]$ values extracted from the defect model (fitted to the C_{chem} data as discussed later). The first point to note is the replication of features discussed in Figure 3, particularly the clear peak in C_{chem}, visible for data above 550 °C and the power law dependences. Good agreement between predicted and measured data is observed, though above 700 °C, only the shapes of the curves remain in good agreement, with an approximate 60% deviation of the model from the data. In this high temperature region, the PCO impedance spectra deviated from the ideal case in Figure 1 for, at present, unknown reasons. As a result, the data for these two temperatures are not discussed further in this paper.

3.4. Estimation of non-stoichiometry

A key objective of this study is to demonstrate the ability to extract oxygen non-stoichiometry of a thin film using chemical capacitance. In order to obtain absolute values for δ at any given temperature and pO_2, using Equation (11), the absolute value of non-stoichiometry, $[V_O^{\bullet\bullet}](pO_2^{\circ})$, must be known at some reference oxygen partial pressure pO_2°. Fortunately, reliable reference values for $[V_O^{\cdot\cdot}]$ can be obtained directly from measurements of C_{chem} as described in the following.

Considering defect region III, in Figure 3, nearly all of the Pr ions are oxidized to Pr^{4+}, thus

$$[Pr_{Ce}^{\times}] \approx [Pr_{Ce}]_{total} \tag{14}$$

Substituting Equations (14) and (3) into Equation (2), and solving for $[V_O^{\cdot\cdot}]$ leads to

$$[V_O^{\bullet\bullet}] = \left(\frac{1}{4} K_{r,Pr}[Pr_{Ce}]_{total}^2[O_O^{\times}]\right)^{1/3} pO_2^{-1/6} \tag{15}$$

Substituting this into the definition of chemical capacitance, Equation (10), one obtains an expression showing the predicted pO_2 dependence of C_{chem}.

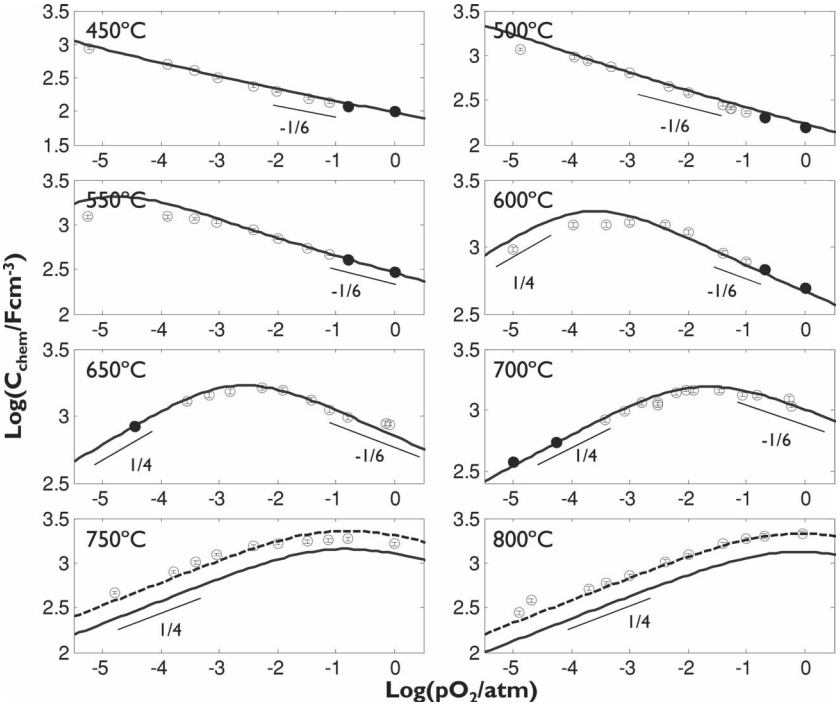

Figure 4. Isothermal dependence of volume-specific C_{chem} (circles) on pO_2, obtained from a symmetric PCO/YSZ/PCO cell with PCO film thickness of 113 nm. The filled circles indicate capacitances used to derive absolute stoichiometry using Equation (17) and Equation (22). Solid lines represent modeled data and dashed lines, for 750 and 800 °C, are 1.6 times the modeled data.

$$C_{\text{chem}} = \frac{4}{3}\frac{q^2 V_{\text{film}}}{kT}\left(\frac{1}{4}K_{r,\text{Pr}}[\text{Pr}_{\text{Ce}}]_{\text{tot}}^2[\text{O}_{\text{O}}^{\times}]\right)^{1/3} pO_2^{-1/6} \quad (16)$$

Noting the definition for $[V_O^{\bullet\bullet}]$ in Equation (15), and substituting this back into Equation (16) leads to

$$C_{\text{chem}} = \frac{4}{3}\frac{q^2 V_{\text{film}}}{kT}[\text{V}_{\text{O}}^{\bullet\bullet}] \quad (17)$$

This approach allows a direct measure of $[V_O^{\bullet\bullet}]$ at any pO_2 from a measurement of C_{chem} with only knowledge of film volume and total Pr concentration as long as the approximation in Equation (14) is valid. Such experimentally derived values can then be used as the reference $[\text{V}_{\text{O}}^{\bullet\bullet}](pO_2^{\circ})$ in Equation (11). Examining Figure 4, the datasets below 700 °C clearly exhibit the $C_{\text{chem}} \propto pO_2^{-1/6}$ regime, allowing the extraction of $[\text{V}_{\text{O}}^{\bullet\bullet}](pO_2^{\circ})$ directly from C_{chem} using Equation (17).

Turning to low pO_2 (region I), where nearly all the Pr is reduced to Pr'_{Ce}, the charge neutrality equation (Equation (3)) can be approximated by:

$$[\text{Pr}'_{\text{Ce}}] = 2[\text{V}_{\text{O}}^{\bullet\bullet}] \approx [\text{Pr}_{\text{Ce}}]_{\text{tot}} \quad (18)$$

Though in this region Pr exists largely as Pr'_{Ce}, a small concentration of $\text{Pr}_{\text{Ce}}^{\times}$ remains, with its concentration derived by substituting Equation (3) into Equation (4), yielding:

$$[\text{Pr}_{\text{Ce}}^{\times}] \approx [\text{Pr}_{\text{Ce}}]_{\text{tot}} - 2[\text{V}_{\text{O}}^{\bullet\bullet}] \quad (19)$$

Substituting $[\text{Pr}_{\text{Ce}}]_{\text{tot}}$ for $[V_O^{\bullet\bullet}]$ and $[\text{Pr}'_{\text{Ce}}]$ using Equation (18) and the r.h.s. of Equation (19) for $[\text{Pr}_{\text{Ce}}{}^{\times}]$ into Equation (2), and solving for $[V_O^{\bullet\bullet}]$ leads to:

$$[\text{V}_{\text{O}}^{\bullet\bullet}] = \frac{[\text{Pr}_{\text{Ce}}]_{\text{tot}}}{2} - \frac{1}{2}\left(\frac{1/2[\text{Pr}_{\text{Ce}}]_{\text{tot}}^3 pO_2^{1/2}}{K_{r,\text{Pr}}[\text{O}_{\text{O}}^{\times}]}\right)^{1/2} \quad (20)$$

Substituting this result into the definition of chemical capacitance, Equation (10), one obtains an expression showing the predicted pO_2 dependence of C_{chem}

$$C_{\text{chem}} = \frac{q^2 V_{\text{film}}}{kT}\left(\frac{1/2[\text{Pr}_{\text{Ce}}]_{\text{tot}}^3}{K_{r,\text{Pr}}[\text{O}_{\text{O}}^{\times}]}\right)^{1/2} pO_2^{1/4} \quad (21)$$

Noting the definition for $[V_O^{\bullet\bullet}]$ in Equation (20), and substituting this back into Equation (21) leads to

$$C_{chem} = \frac{q^2 V_{\text{film}}}{kT}\left([\text{Pr}_{\text{Ce}}]_{\text{tot}} - 2[\text{V}_{\text{O}}^{\bullet\bullet}]\right) \quad (22)$$

The $C_{\text{chem}} \propto pO_2^{1/4}$ dependence is clearly visible in Figure 4 for temperatures above 650 °C, allowing the extraction of $[\text{V}_{\text{O}}^{\bullet\bullet}](pO_2^{\circ})$ directly from a measurement of C_{chem} using Equation (22). One last point worth mentioning here, is that in the above derivation, the dependence of $H_{r,\text{Pr}}$ on δ was assumed negligible (see Equation (6)), a valid approximation considering the relatively small changes in $[V_O^{\bullet\bullet}]$ in regions I and III and confirmed by the observation of 1/4 and –1/6 power laws in Figure 4. Once δ was extracted in region II using Equation (11), the defect equilibria model was fit to all values of δ using the dependence of $H_{r,\text{Pr}}$ on δ given by Equation (6).

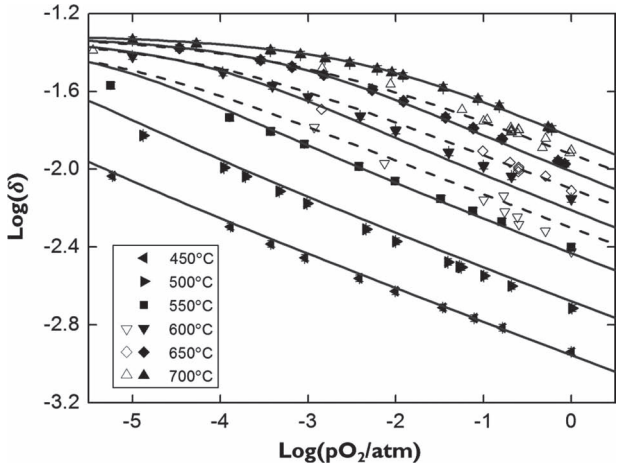

Figure 5. Non-stoichiometry of thin film and bulk PCO derived from C_{chem} (filled symbols) and TGA (empty symbols), respectively.[18] The solid and dashed lines represent δ for thin films and bulk, respectively, calculated from the defect model using the parameters listed in Table 1. Error bars (shown) for non-stoichiometry are smaller than the size of the data points.

Figure 5 shows the absolute values of δ extracted from C_{chem} as a function of pO_2 for a series of isotherms, derived by application of Equation (11) and with further aid of either Equations (17) or (22). These results are compared with data obtained for bulk PCO measured by TGA as well as values calculated from the defect model using the parameters listed in **Table 1**. First, one notes that δ derived from C_{chem} show less scatter than those derived from TGA measurements. Second, the experimental data agree well with the trends and absolute values observed for the defect model, derived by fitting δ for the film, demonstrating the utility of chemical capacitance to derive reliable non-stoichiometry data for ceria based thin films. At the same time, the film exhibits a small but systematic shift from the bulk data in the direction of larger δ values for the same temperature and pO_2 conditions.

By fitting the PCO defect model to the δ values extracted from C_{chem}, the parameters used in the defect equilibria models, see Table 1, were derived. One observes that the parameters derived from the thin film chemical capacitance data are close to values derived for bulk $\text{Pr}_{0.1}\text{Ce}_{0.9}\text{O}_{2-\delta}$. It is interesting to note that the enthalpy for reduction, while nominally smaller for the film, is equal to that of the bulk taking into account the margin of

Table 1. Parameters used in the defect equilibria model for $\text{Pr}_{0.1}\text{Ce}_{0.9}\text{O}_{2-\delta}$.

Morphology	$H_{r,\text{Pr}}^{\circ}$ [eV]	$k_{r,\text{Pr}}^{\circ}$ [atm$^{1/2}$]	f [eVδ^{-1}]	$[\text{Pr}_{0.1}\text{Ce}_{0.9}\text{O}_{2-\delta}]$ [cm^{-3}]
Thin film (present work)	1.80 ± 0.04[a)]	$(0.90 \pm 0.60)\times10^{6}$ [a)]	-6.2 ± 1.5[a)]	2.52×10^{22}[c)]
Bulk	1.90 ± 0.07[b)]	$(2.114 \pm 1.23)\times10^{6}$[b)]	-4.63 ± 1.9[b)]	2.52×10^{22}[c)]

[a)]Determined from defect equilibria (C_{chem}); [b)]Determined from defect equilibria (TGA);[18] [c)]For density = 7.21 g·cm^{-3}.[18]

error reported for the two values. From these results, one would conclude that the thermodynamic parameters for PCO change little with respect to the bulk, within experimental error, when prepared in the present thin film geometry.

The question remains why bulk and thin film non-stoichiometry data match well for ceria thin films but not for the mixed conducting perovskites $La_{1-x}Sr_xCoO_{3-\delta}$ reported to date. For example, Kawada et al. reported a 45% increase in reduction enthalpy for LSC, whereas in the present case only a 5% decrease, within the margin of error, is observed here for PCO.[11] While others have suggested that strain, induced either by lattice mismatch or thermal expansion mismatch between substrate and film, may be playing a role,[11] an alternate explanation, based on the known reactivity of many of the perovskite oxide films with YSZ,[27] may be a more likely reason. Along these lines, one may also note the heavy segregation of Sr to the surfaces of the perovskite films, leading to large compositional changes, at least in the vicinity of the surface.[8,28] To date, no evidence for significant Pr segregation to the surface in PCO, nor reaction with the YSZ substrate, has been observed, nor is expected.

4. Summary and Conclusions

The chemical capacitance of $Pr_{0.1}Ce_{0.9}O_{2-\delta}$ (PCO) thin films, deposited onto single crystal YSZ substrates, was extracted from impedance data and used to obtain values for δ as a function of temperature and pO_2. Thermodynamic parameters, describing defect generation in PCO, were derived and found to be in close agreement with those obtained for bulk PCO, demonstrating the utility of chemical capacitance for deriving reliable non-stoichiometry data for ceria based thin films. Approximations, relating chemical capacitance directly to oxygen vacancy concentration, without a fitting parameter (as used in previous studies), were derived in key defect regimes, thus allowing extraction of the absolute values of δ for specific ranges of pO_2 and temperature. Poor correlations found in earlier studies between chemical capacitance and TGA or coulometrically derived values for δ in perovskite films may be due to chemical reactions between the perovskite films and the underlying YSZ substrate or compositional changes in the films related to segregation effects. Future studies on these materials should carefully examine the film/substrate and film/gas interfaces to ensure that they are compositionally correct.

While the properties of functional oxide thin films often depend strongly on their oxygen stoichiometry, there have been few ways to extract this information reliably and in situ until this time. Evaluation of oxygen non-stoichiometry by chemical capacitance should be able to provide this critical information, as demonstrated in this study. Our group plans to test the generality of these observations on PCO thin films by performing similar studies on other types of oxide films.

5. Experimental Section

Sample Preparation and Characterization: Details of $Pr_{0.1}Ce_{0.9}O_{2-\delta}$ film preparation are discussed elsewhere;[17] a summary is given here. Films were deposited onto (001) oriented single crystal YSZ (8 mol% Y_2O_3 stabilized) substrates (10 mm × 10 mm × 0.5 mm; MTI Corporation, Richmond, CA) by pulsed laser deposition (PLD) from oxide targets. The film structure was analyzed by X-ray diffraction (XRD; X'Pert PRO MPD, PANalytical) with approximate grain size and surface roughness determined by atomic force microscopy (Digital Instruments Nanoscope IIIa) and film thickness determined by surface profilometry (KLA-Tencor P-16+ stylus profiler).

Electrical and Electrochemical Measurement: Two different cell geometries were prepared for IS measurements: a symmetrical structure with identically sized (9 mm × 9 mm) PCO electrodes on both sides of the YSZ electrolyte, and an asymmetrical structure of 1–10 mm diameter PCO working electrodes with porous Ag counter electrodes (SPI Silver Paste Plus, SPI Supplies, Chester, PA, USA) on the opposite side of the YSZ substrate/electrolyte. In both configurations, Au paste (Fuel cell materials, Lewis Center, Ohio), serving as current collector, was applied to the top surface of the PCO electrode. The IS measurements were performed at temperatures between 450 and 800 °C and oxygen partial pressures between 10^{-5} and 1 atm, controlled by mixing N_2 and O_2 with the aid of mass flow controllers (MKS) and monitored by an in situ YSZ Nernst type oxygen sensor. IS measurements, covering the frequency range from 0.032 Hz to 1 MHz, with AC amplitude of 20 mV, were performed using an impedance analyzer (Solartron 1260) and fit with equivalent circuits using Zview and Zplot software (Scribner Associates).

Data Fitting: Data fitting to defect models to obtain thermodynamic parameters was performed using Matlab (Mathworks). Parameters in the models were determined using the Gauss–Newton method of nonlinear regression with partial derivatives approximated numerically.[29] Initial estimations were refined visually and then regression was performed in a step-wise iterative manner. Error estimates for modeled parameters are reported for an approximate 95% confidence interval of the regressed model.

Acknowledgements

This work was supported by the National Science Foundation Materials World Network in collaboration with Prof. Moos, Universität Bayreuth, Germany under grant No. DMR-0908627. Partial support was also received from Basic Energy Sciences, Department of Energy under award DE-SC0002633. The authors thank Mr. Jae Jin Kim for preparation of the PLD targets. S.R.B. gratefully recognizes support from I^2CNER, established and supported by the World Premier International Research Center Initiative (WPI), MEXT, Japan.

Received: July 26, 2012
Revised: October 9, 2012
Published online: November 26, 2012

[1] Y. Min, H. L. Tuller, S. Palzer, J. Wöllenstein, H. Böttner, *Sens. Actuators, B* **2003**, *93*, 435.
[2] S. M. Haile, *Acta Mater.* **2003**, *51*, 5981.
[3] J. L. M. Rupp, B. Scherrer, N. Schäuble, L. J. Gauckler, *Adv. Funct. Mater.* **2010**, *20*, 2807.
[4] J. Fleig, F. S. Baumann, V. Brichzin, H. R. Kim, J. Jamnik, G. Cristiani, H. U. Habermeier, J. Maier, *Fuel Cells* **2006**, *6*, 284.
[5] W. Jung, H. L. Tuller, *Solid State Ionics* **2009**, *180*, 843.
[6] T. Suzuki, *Solid State Ionics* **2002**, *151*, 111.
[7] X. X. Guo, J. Maier, *Adv. Mater.* **2009**, *21*, 2619.
[8] W. Jung, H. L. Tuller, *Energy Environ. Sci.* **2012**, 5370.
[9] H. L. Tuller, S. R. Bishop, *Annu. Rev. Mater. Res.* **2011**, *41*, 369.
[10] H. Seh, H. Fritze, H. L. Tuller, *J. Electroceram.* **2007**, *18*, 139.
[11] T. Kawada, J. Suzuki, M. Sase, A. Kaimai, K. Yashiro, Y. Nigara, J. Mizusaki, K. Kawamura, H. Yugami, *J. Electrochem. Soc.* **2002**, *149*, E252.

[12] S. Wang, S. Cho, H. Wang, A. Jacobson, *ECS Trans.* **2011**, *35*, 1891.
[13] G. J. la O', S.-J. Ahn, E. Crumlin, Y. Orikasa, M. D. Biegalski, H. M. Christen, Y. Shao-Horn, *Angew. Chem. Int. Ed.* **2010**, *49*, 5344.
[14] T. Nakamura, K. Yashiro, A. Kaimai, T. Otake, K. Sato, T. Kawada, J. Mizusaki, *J. Electrochem. Soc.* **2008**, *155*, B1244.
[15] W. C. Chueh, S. M. Haile, *Phys. Chem. Chem. Phys.* **2009**, *11*, 8144.
[16] G. T. Kim, S. Wang, A. J. Jacobson, Z. Yuan, C. Chen, *J. Mater. Chem.* **2007**, *17*, 1316.
[17] D. Chen, S. Bishop, H. L. Tuller, *J. Electroceram.* **2012**, *28*, 62.
[18] S. R. Bishop, T. S. Stefanik, H. L. Tuller, *Phys. Chem. Chem. Phys.* **2011**, *13*, 10165.
[19] S. B. Adler, *Chem. Rev.* **2004**, *104*, 4791.
[20] C. Chatzichristodoulou, P. V. Hendriksen, A. Hagen, *J. Electrochem. Soc.* **2010**, *157*, B299.
[21] S. R. Bishop, T. S. Stefanik, H. L. Tuller, *J. Mater. Res.* **2012**, *27*, 2009.
[22] J. Jamnik, J. Maier, *Phys. Chem. Chem. Phys.* **2001**, *3*, 1668.
[23] W. Lai, S. M. Haile, *J. Am. Ceram. Soc.* **2005**, *88*, 2979.
[24] J. Fleig, *Solid State Ionics* **2002**, *150*, 181.
[25] F. S. Baumann, J. Fleig, G. Cristiani, B. Stuhlhofer, H.-U. Habermeier, J. Maier, *J. Electrochem. Soc.* **2007**, *154*, B931.
[26] W. Jung, H. L. Tuller, *J. Electrochem. Soc.* **2008**, *155*, B1194.
[27] S. P. Jiang, *J. Mater. Sci.* **2008**, *43*, 6799.
[28] G. J. la O', R. F. Savinell, Y. Shao-Horn, *J. Electrochem. Soc.* **2009**, *156*, B771.
[29] S. Chapra, R. Canale, *Numerical Methods for Engineers*, McGraw-Hill, Inc., Boston **2005**.